AGU PUBLICATIONS

JGR

Journal of Geophysical Research: Space Physics

RESEARCH ARTICLE
10.1002/2016JA023067

Key Points:
- Electron fluxes decrease after Pdyn peak in northward IMF B_z, while dropouts occur during Pdyn pulse under southward IMF B_z
- Deeper earthward magnetopause erosion can lead to prompt flux dropout at L ~ 5
- The events with high electron fluxes before the Pdyn pulse tend to experience more severe electron flux dropouts

Correspondence to:
B. Ni,
bbni@whu.edu.cn

Citation:
Ni, B., Z. Xiang, X. Gu, Y. Y. Shprits, C. Zhou, Z. Zhao, X. Zhang, and P. Zuo (2016), Dynamic responses of the Earth's radiation belts during periods of solar wind dynamic pressure pulse based on normalized superposed epoch analysis, *J. Geophys. Res. Space Physics*, *121*, 8523–8536, doi:10.1002/2016JA023067.

Received 14 JUN 2016
Accepted 22 AUG 2016
Accepted article online 26 AUG 2016
Published online 17 SEP 2016

Dynamic responses of the Earth's radiation belts during periods of solar wind dynamic pressure pulse based on normalized superposed epoch analysis

Binbin Ni[1,2], Zheng Xiang[1], Xudong Gu[1], Yuri Y. Shprits[3], Chen Zhou[1], Zhengyu Zhao[1], Xianguo Zhang[2], and Pingbing Zuo[2]

[1]Department of Space Physics, School of Electronic Information, Wuhan University, Wuhan, China, [2]State Key Laboratory of Space Weather, National Space Science Center, Chinese Academy of Sciences, Beijing, China, [3]GFZ German Research Center for Geosciences, Potsdam, Germany

Abstract Using the electron flux measurements obtained from five satellites (GOES 15 and POES 15, 16, 18, and 19), we investigate the flux variations of radiation belt electrons during forty solar wind dynamic pressure pulses identified between September 2012 and December 2014. By utilizing the mean duration of the pressure pulses as the epoch timeline and stretching or compressing the time phases of individual events to normalize the duration by means of linear interpolation, we have performed normalized superposed epoch analysis to evaluate the dynamic responses of radiation belt energetic electrons corresponding to various groups of solar wind and magnetospheric conditions in association with solar wind dynamic pressure pulses. Our results indicate that by adopting the timeline normalization we can reproduce the typical response of the electron radiation belts to pressure pulses. Radiation belt electron fluxes exhibit large depletions right after the P_{dyn} peak during the periods of northward interplanetary magnetic field (IMF) B_z and are more likely to occur during the P_{dyn} pulse under southward IMF B_z conditions. For the pulse events with large negative values of $(Dst)_{min}$, radiation belt electrons respond in a manner similar to those with southward IMF B_z, and the corresponding postpulse recovery can extend to $L \sim 3$ and exceed the prepulse flux levels. Triggered by the solar wind pressure enhancements, deeper earthward magnetopause erosion provides favorable conditions for the prompt electron flux dropouts that extend down to $L \sim 5$, and the pressure pulses with longer duration tend to produce quicker and stronger electron flux decay. In addition, the events with high electron fluxes before the P_{dyn} pulse tend to experience more severe electron flux dropouts during the course of the pulse, while the largest rate of electron flux increase before and after the pulse occurs under the preconditioned low electron fluxes. These new results help us understand how electron fluxes respond to solar wind dynamic pressure pulses and how these responses depend on the solar wind and geomagnetic conditions and on the preconditions in the electron radiation belts.

1. Introduction

Radiation belt electron fluxes show variations on various timescales, and understanding of the radiation belt dynamic responses to solar wind driving forces remains one central problem of the magnetospheric physics, since extreme geospace radiation environment can pose potentially severe damage to satellites and astronauts [*Baker et al.*, 2004]. Electron flux dropouts present one of the most dramatic changes in the radiation belts. As defined by *Turner et al.* [2012a], a dropout indicates that the electron flux decreases by at least a factor of 50 (or by less than 50 if the flux level drops from some significant level to the instrumental background/noise level) as measured at approximately the same L shell, equatorial pitch angle, and magnetic local time by the same spacecraft in a period less than 24 h. Usually, electron flux dropouts can occur over a broad range of energy (tens of keV up to several MeV) and L shell (i.e., $L > \sim 3$).

It has been widely accepted that both losses to the atmosphere due to wave-induced pitch angle scattering and to the magnetopause due to magnetospheric compression by enhanced solar wind activity play significant roles in producing electron flux dropouts; however, their relative contributions remain not fully resolved. On one hand, a variety of magnetospheric waves, including whistler-mode chorus, plasmaspheric hiss, electromagnetic ion cyclotron (EMIC) waves, and magnetosonic waves, can impact the dynamics of radiation belt electrons via wave-particle interactions [e.g., *Shprits et al.*, 2008a, 2008b; *Thorne*, 2010; *Ni et al.*, 2013b, 2015; *Xiang et al.*, 2016]. These emissions interact with magnetospheric electrons at energies ranging from ~ keV to ~ 10 MeV

and force the electrons to experience precipitation loss to the atmosphere through pitch angle diffusion, while the corresponding loss timescales vary from minutes to days. On the other hand, the magnetospheric compression due to enhanced solar wind dynamic pressure (P_{dyn}) substantially depletes electron fluxes around the outer boundary at high L shells where the electrons find themselves moving from a closed to open drift shell during the geomagnetic disturbance. *Shprits et al*. [2006] noticed that electron flux dropouts are correlated with both P_{dyn} increases and magnetopause compressions. They suggested that the inward gradients created by the loss to the magnetopause can drive the outward radial diffusion and produce dropouts down to lower L values. Their radial diffusion simulations showed that dropouts can occur down to $L \sim 4$ and reproduce the observed dynamics of radiation belt electron fluxes. They also showed that dropouts were observed at energies down to 100 keV on highly elliptical orbit satellite observations, which cannot be explained by EMIC wave-induced losses. *Turner et al*. [2012b] provided further observational evidence of this loss mechanism by showing that low-altitude orbiting NOAA POES spacecraft did not observe the atmospheric precipitation for an event when the dropout was clearly seen in the trapped electron fluxes. *Hwang et al*. [2015] analyzed an electron flux dropout event during a weak storm on 7–8 November 2008, by combining the multisatellite measurements with the Radiation Belt Environment model simulations [*Fok et al*., 2008], to show that the electron flux dropout could be dominated by a combination of magnetopause shadowing and/or atmospheric loss.

While *Shprits et al*. [2006] considered only individual events, *Shprits et al*. [2012] and *Ni et al*. [2013a], using data-assimilative reconstruction of the radiation belt dynamics [e.g., *Ni et al*., 2009a, 2009b] from multiple spacecraft for statistical analyses, found that 81% of the electron phase space density dropouts are related to moderate increase or sudden jump in the solar wind dynamic pressure and that 68% of identified solar wind dynamic pressure pulses correspond to electron phase space density dropout events. Applying superposed epoch analysis to relativistic electron fluxes measured by Solar Anomalous and Magnetospheric Particle Explorer (SAMPEX), *Yuan and Zong* [2013] showed that statistically high solar wind dynamic pressure leads to larger electron flux dropouts than low dynamic pressure and that southward interplanetary magnetic field (IMF) results in stronger flux decreases compared with northward IMF. A following study of *Hietala et al*. [2014] adopted the method of normalized superposed epoch analysis to find that interplanetary coronal mass ejection (ICME)-driven sheaths typically produce more than an order of magnitude decrease in the relativistic electron fluxes and that the fluxes can stay below the preevent level for > 2 days after the sheath passage, resulting from enhanced radial diffusion under magnetospheric compression conditions. Since their study applied a 24 h sliding window average to the flux observations, the start time of the electron flux reduction was undefined and the variations faster than 1 day were omitted, which however can provide important clues of the underlying physics. For instance, if the effect of magnetopause shadowing and successive outward transportation controls the dropout of electron fluxes, the fluxes near the heart of the outer zone (i.e., $L \sim 4$) are very likely to decrease when the magnetopause undergoes outward mitigation rather than during its inward penetration. If localized wave-particle interactions, such as EMIC wave-induced pitch angle diffusion, dominate, it is expected that the relativistic electron flux dropout at $L \sim 4$ can occur rapidly on timescales of minutes to hours.

By averaging along the epoch timeline to remove the influence of random noise and to reveal the typical time series for the specific classification of events, superposed epoch analysis is commonly used to describe the most likely dynamic behavior of the radiation belts in response to evolving solar wind conditions. As far as we are aware, compared to the conventional technique of superposed epoch analysis that defines a single epoch marker, normalized superposed epoch analysis has not been adopted yet to explore the dynamic responses of the radiation belts to solar wind dynamic pressure pulses, while the latter uses multiple references in each event to normalize the timeline and possesses the advantage of placing all of the driver features on a similar timeline with respect to the critical moments during events [*Yokoyama and Kamide*, 1997; *Katus et al*., 2013]. The methodology of normalized superposed epoch analysis allows us to include events of specific interest which occur at different timescales. Therefore, the present study is dedicated to implementing normalized superposed epoch analysis to long-term data sets from GOES and POES satellites in order to elaborate the dynamic responses of Earth's radiation belts during periods of solar wind dynamic pressure pulse and shed light on the underlying physical connection(s). We give the description of the data and methodology in section 2. Section 3 shows the normalized superposed epoch analysis results for 40 solar wind dynamic pressure pulses identified during the period from September 2012 to December 2014. A number of classifications of pressure pulse event and radiation belt electron dynamics are selected to explore the major features and their potential correlation with solar wind / magnetospheric parameters. We discuss the results in section 4 and make conclusions in section 5.

2. Data and Methodology

The electron flux measurements collected from five satellites, including the geosynchronous GOES 15 satellite and Sun-synchronous, low-altitude POES 15, 16, 18, and 19 satellites, are adopted for the present study. The particle detector on board GOES 15 can provide 1 min resolution data of electron fluxes at three energy channels, i.e., $>$ 0.8 MeV, $>$ 2 MeV, and $>$ 4 MeV, at the geostationary orbit. Medium Energy Proton and Electron Detector (MEPED) on board four POES satellites measure both trapped and precipitated electron fluxes in three energy bands, i.e., $>$30 keV, $>$100 keV, and $>$300 keV, at the altitude of ~ 800 km with an orbital period of ~ 100 min [*Evans and Greer*, 2004; *Green*, 2013]. To obtain the data sets as cleanly as possible, we have removed the proton contamination using the correction procedure described in *Lam et al.* [2010] and also deleted from the database the observation points during the solar proton events and those measured at the region of the South Atlantic anomaly (SAA) [*Casadio and Arino*, 2011]. The data of solar wind parameter and geomagnetic indices are directly acquired from the online OmniWeb (http://omniweb.gsfc.nasa.gov/) with a time resolution of 1 h. With the above data available, we then identify the events of solar wind dynamic pressure pulse during the period from September 2012 to December 2014. The criterion of a solar wind dynamic pressure pulse is that the magnitude of the pressure increases by 5 nPa within 5 h [e.g., *Shprits et al.*, 2012; *Ni et al.*, 2013a]. By a careful vision check, we finally establish a robust database of 40 solar wind dynamic pressure pulses with good quality in situ electron flux data for the subsequent investigation. The details of each identified pressure pulse event are listed in Table 1. It is worthwhile to note that we delete 15 dynamic pressure pulse events either due to the serious gap in satellites data or the close proximity of two neighboring events (less than 24 h).

In contrast to the conventional method of superposed epoch analysis featured by the adoption of one single epoch marker [*Borovsky and Denton*, 2009], in this study we perform normalized superposed epoch analysis by adopting two epoch markers, i.e., the onset of solar wind dynamic pressure pulse as the first epoch marker and its peak as the second marker. The onset of a solar wind dynamic pressure pulse is identified at the time of low P_{dyn} value which is or closely approaches the prepulse level (usually $<$ 3 nPa). To study the responses of radiation belt electron fluxes during a standard solar wind dynamic pressure pulse, the mean duration of each pulse is utilized to normalize the epoch timeline. By normalizing the time period during each superposed epoch in terms of linear interpolation, the individual phases of the pressure pulse of interest are essentially either stretched or compressed to the average duration of the 40 pulse events between the two epoch markers. For the sake of time consistency, the temporal variation of electron flux data from GOES 15 is normalized in the same method of linear interpolation on the basis of average pulse duration. For electron flux data from POES satellites, we first apply bin averaging every 30 min (~ a fourth of the orbital period) times every 0.1 L shell to acquire the radial profile of radiation belt electron fluxes and then normalize its temporal variation upon the mean epoch timeline of the pressure pulse. We also carefully check the normalization results to assure that the major features of radiation belt electron dynamic responses to each pulse event are reasonably retained. Normalized superposed epoch analysis can provide insight into a time interval of interest rather than a time epoch only, thereby holding the nature to reproduce the average features of considered events in a more informative manner.

Figure 1 displays an example of the solar wind dynamic pressure pulse and prepulse to postpulse variations of radiation belt electron fluxes observed by GOES and POES satellites during the 3 day period from 7 December to 9 December 2013. The red curve in the third panel represents the duration of identified solar wind dynamic pressure pulse (P_{dyn}). On 7 December, the dynamic pressure began to increase at 17 UT. The magnetopause location (the fourth panel), obtained based on the model of *Shue et al.* [1997], moved inward quickly, while the electron fluxes showed only a slight change in the GOES (the fifth panel) and POES (the sixth to eighth panels) observations. As the dynamic pressure continued to increase at a faster rate, reaching the peak value of 16 nPa in 6 h, IMF B_z shifted from northward to southward, and the magnetopause penetrated deeper to lower L shells. Accordingly, the GOES electron fluxes of $>$ 0.6 MeV and $>$ 2.0 MeV channels declined quickly. At 02 UT on 8 December, when the dynamic pressure reached its maximum and the magnetopause approached L ~ 7, the GOES electron fluxes dropped substantially compared to the levels at 00 UT (2 h before) by about 3 orders of magnitude for $>$ 0.6 MeV electrons and by over 1 order of magnitude for $>$ 2.0 MeV electrons. Following the peak of the dynamic pressure, the magnetopause started to move outward. Fluxes of $>$ 0.6 MeV electrons continued to reduce for a few hours, while $>$ 2.0 MeV electron fluxes remained almost unchanged at a very low level. Meanwhile, POES measurements indicated that the fluxes of three energy channels increased considerably

Table 1. List of Solar Wind Dynamic Pressure Pulses From September 2012 to December 2014

No.	Start Time YYYY-MM-DD	End Time YYYY-MM-DD	Duration (h)	P_{dyn} (nPa) Max	IMF B_z (nT) Mean	MP Min	*Dst* (nT) Min	GOES Dropout Index[a]
01	2012-9-3/11:00	2012-9-3/14:00	3	10.2	−1.5	7.2	−78	0.06
02	2012-9-4/22:00	2012-9-5/05:00	7	7.6	−2.3	8.5	−70	0.22
03	2012-9-30/19:00	2012-10-1/00:00	5	7.5	−5.4	6.6	−133	0.07
04	2012-10-31/14:00	2012-10-31/16:00	2	7.6	−1.4	8.2	−74	0.01
05	2012-11-12/14:00	2012-11-13/00:00	10	10.5	−1.7	7.5	−109	0.18
06	2012-11-23/21:00	2012-11-24/00:00	3	8.6	−4	8.1	−42	0.01
07	2013-1-18/11:00	2013-1-18/13:00	2	14.9	11.1	7	−53	0.18
08	2013-3-1/05:00	2013-3-1/10:00	5	8.7	−3.1	7.8	−55	0.44
09	2013-3-17/05:00	2013-3-17/08:00	3	12.5	−1.1	6.7	−132	0.25
10	2013-3-23/17:00	2013-3-23/23:00	6	8.5	−0.4	8.3	−32	0.02
11	2013-4-23/22:00	2013-4-24/04:00	6	9.7	−5.1	7.5	−49	0.29
12	2013-5-18/00:00	2013-5-18/02:00	2	6.9	−3.4	7.8	−57	0.14
13	2013-5-24/17:00	2013-5-24/19:00	2	9.1	−2	7.9	−55	0.01
14	2013-5-31/14:00	2013-5-31/23:00	9	12.2	−0.3	7	−119	0
15	2013-6-9/23:00	2013-6-10/05:00	6	6.9	−2.7	8.5	−16	0
16	2013-6-27/13:00	2013-6-28/00:00	11	9.5	−1.5	7.7	−98	0
17	2013-8-20/13:00	2013-8-20/23:00	10	8.6	0.3	8.1	−23	0
18	2013-8-27/11:00	2013-8-27/17:00	6	6.6	−1.2	8	−54	0.01
19	2013-9-24/06:00	2013-9-24/12:00	6	7.4	−0.6	8	−24	0.01
20	2013-10-2/01:00	2013-10-2/05:00	4	30.8	−5.4	5.6	−67	0.04
21	2013-10-8/13:00	2013-10-8/22:00	9	12.8	1	7.8	−65	0.02
22	2013-12-7/17:00	2013-12-8/02:00	9	16.1	0.4	7.1	−66	0.04
23	2013-12-13/09:00	2013-12-13/14:00	5	7.9	0.2	8.4	−37	0.07
24	2014-2-7/16:00	2014-2-8/03:00	11	19.2	0.6	6.7	−32	0.07
25	2014-2-15/12:00	2014-2-16/00:00	12	19.5	3.2	6.7	−22	0.01
26	2014-2-19/04:00	2014-2-19/13:00	9	12.2	−7.9	7.5	−102	0.39
27	2014-2-23/02:00	2014-2-23/09:00	7	10.2	3.3	8	−56	0.02
28	2014-2-27/08:00	2014-2-27/20:00	12	12	−1.6	6.7	−99	0.37
29	2014-3-25/19:00	2014-3-25/21:00	2	6.2	−1.1	8.6	−22	0.44
30	2014-4-5/10:00	2014-4-5/22:00	12	13.4	−2.4	7.4	−13	0.32
31	2014-4-19/02:00	2014-4-19/04:00	2	8.8	−2.2	7.8	−17	0.14
32	2014-4-20/10:00	2014-4-20/14:00	4	8.8	6.1	7.8	−24	0.06
33	2014-6-7/16:00	2014-6-8/07:00	15	31.3	1.3	6.8	−38	0.42
34	2014-7-14/06:00	2014-7-14/15:00	9	9.6	7.9	8.2	−14	0.35
35	2014-9-12/15:00	2014-9-12/19:00	4	17.2	9.7	6.7	−75	0.04
36	2014-9-19/00:00	2014-9-19/06:00	6	12.3	−4.7	7.8	−22	0.44
37	2014-10-12/16:00	2014-10-12/21:00	5	9.2	0.3	7.5	−40	0.44
38	2014-11-4/19:00	2014-11-4/21:00	2	10.1	−0.3	7.8	−38	0.04
39	2014-12-21/18:00	2014-12-21/23:00	5	10.3	−5	7.2	−73	0.04
40	2014-12-23/10:00	2014-12-23/12:00	2	10.3	7.3	8.2	−55	0.54

[a]Dropout index indicates the ratio of the minimum of GOES > 2.0 MeV electron flux in the 48 h after zero epoch time to the mean value of GOES > 2.0 MeV electron flux in the 24 h before zero epoch time, which is designed to represent the degree of electron flux depletion at the geostationary orbit.

at $L > \sim 7$ during the period from 21 to 24 UT on 7 December and then dropped substantially with the flux dropouts extending deeply into $L < \sim 4$ along with the rise of the dynamic pressure. Distinct differences in the POES electron flux evolution occur between the lower energy channels (i.e., > 30 keV and > 100 keV) and the higher energy channel (i.e., > 300 keV). It is clear that the degree of the flux dropout corresponding to the pressure pulse increased with electron energy, being most pronounced for > 300 keV electrons. In accordance with the pressure jump and the innermost intrusion of the magnetopause and the plasmapause, > 30 keV and > 100 keV electrons penetrated downward to $L \sim 3$ but > 300 keV electrons did not. It is worthwhile to note that the electron flux dropout took place during the main phase of a modest geomagnetic storm with $(Dst)_{min} \sim -60$ nT. The fluxes of > 30 keV and > 100 keV electrons started to increase right after the $(Dst)_{min}$. At around 09 UT on 8 December, the dynamic pressure almost returned to the prestorm value. Accordingly, the electron fluxes for > 30 keV– > 0.6 MeV energy channels showed the gradual recovery, which distinctly took place first at lower L shells and then expanded to higher L shells. The > 2 MeV electron fluxes exhibited almost no increase until 18 UT on 8 December. Overall, the fluxes for the lower energy channels recovered on a timescale much faster than the higher energy

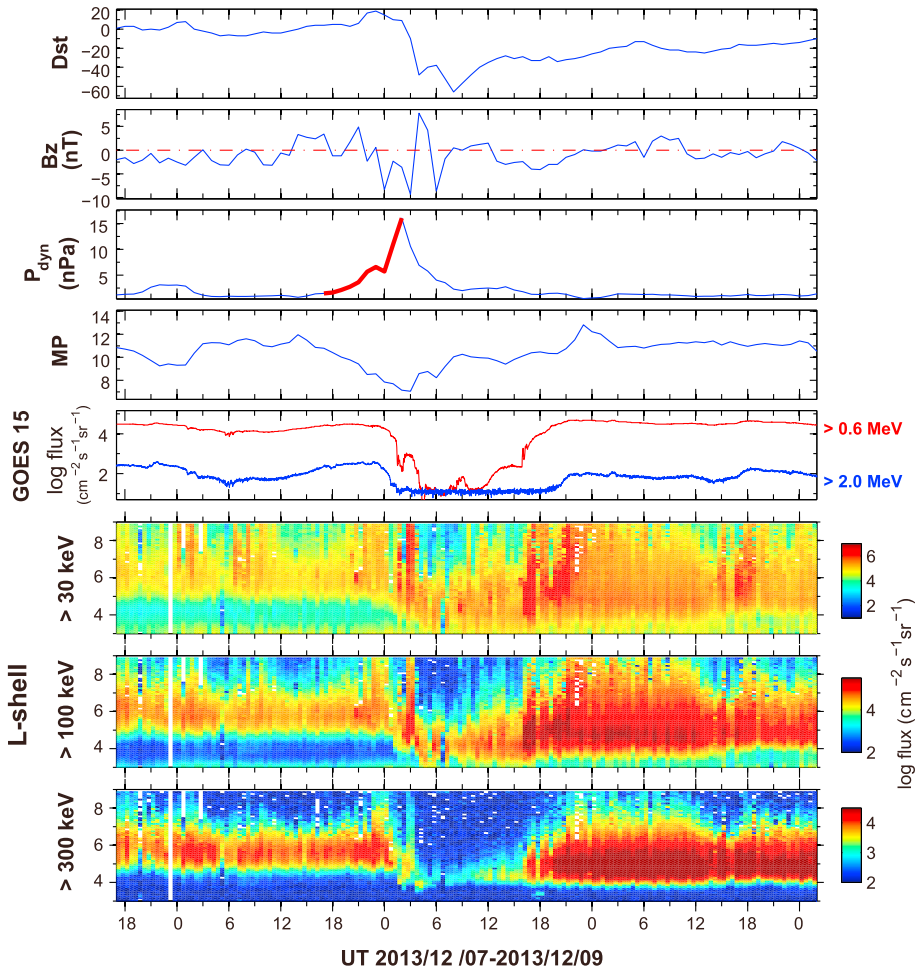

Figure 1. An example event of electron flux dropout during a solar wind dynamic pressure pulse. Time series of OmniWeb geomagnetic indices and solar wind parameters for the 3 day interval between 7 December 2013 and 9 December 2013. (first to eighth panels) *Dst*, IMF B_z, solar wind dynamic pressure (P_{dyn}), the magnetopause standoff distance modeled following *Shue et al.* [1997], observations of radiation belt electron fluxes at the geostationary orbit by GOES 15 satellite for two energy channels: (red) > 0.6 MeV, (blue) > 2.0 MeV, temporal variations of radiation belt trapped electron fluxes observed by four POES (15, 16, 18, and 19) satellites for three energy channels (>30 keV, > 100 keV, and > 300 keV), which are binned by 0.1 *L* times 0.5 h. In Figure 1 (third panel) of P_{dyn}, the overplotted red curve marks the P_{dyn} rise period.

channels. Such an energy dispersive feature of radiation belt electron flux evolution in response to the dynamic pressure pulse becomes even more striking when checking together the measurements of POES and GOES at different electron energy channels from > 30 keV to > 2 MeV.

The example of Figure 1 clearly depicts the significant impact of solar wind dynamic pressure pulse on the radiation belt electron dynamics and the delicate spatiotemporal variations of radiation belt electron fluxes during and after the course of a dynamic pressure pulse. To investigate in detail the impact on radiation belt electron flux variations under various solar wind conditions, 40 solar wind dynamic pressure events are carefully selected to form five representative groups for quantitative comparisons on basis of the following criteria: (1) 10 events with largest average northward IMF B_z versus 10 events with largest average southward IMF B_z (the time range of averaging IMF B_z is the period of the normalized pulse); (2) 10 events with lowest magnetopause position versus 10 events with highest magnetopause position; (3) 10 events with smallest values of $(Dst)_{min}$ versus 10 events with largest values of $(Dst)_{min}$;(4) 10 events with smallest dropout index of GOES > 2.0 MeV electron fluxes versus 10 events with largest dropout index of GOES > 2.0 MeV electron fluxes; and (5) 10 events with longest P_{dyn} rise time versus 10 events with shortest P_{dyn} rise time.

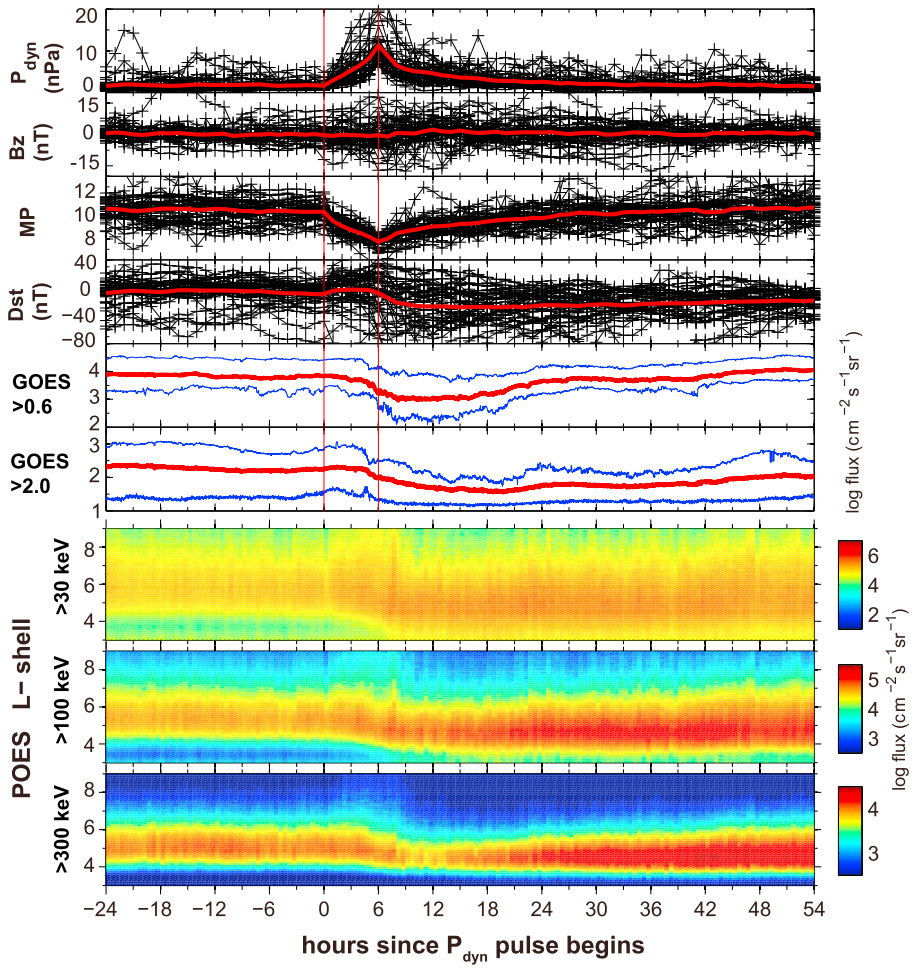

Figure 2. Normalized superposed epoch analysis results of all 40 events. (first to ninth panels) P_{dyn}, IMF B_z, MP, *Dst*, electron fluxes observed by GOES 15, and bin-averaged trapped electron fluxes observed by four POES satellites. In Figure 2 (first to fourth panels), the black curves with markers (+) show the parameter data for each event, and the red thick lines represent the mean values. In Figure 2 (fifth and sixth panels), the red lines are the mean values, and the blue lines are the upper and lower quartile levels for electron fluxes.

3. Analysis Results

Figure 2 presents the results of the normalized superposed epoch analysis for all 40 dynamic pressure pulse events tabulated in Table 1. Figure 2 (first to fourth panels) presents the temporal variations of solar wind dynamic pressure P_{dyn}, interplanetary magnetic field (IMF) B_z, magnetopause standoff distance, and the *Dst* index from 24 h preceding to 48 h following the solar wind dynamic pressure pulse. The two vertical red lines indicate the normalized 6 h duration of the identified solar wind dynamic pressure pulse after either stretching or compression over time. Note that 6 h is the average duration for all considered 40 pressure pulse events. In Figure 2 (first to fourth panels), the black curves with markers (+) show the parameter data for each event and the thick red curves represent the mean values for all 40 events. Figure 2 (fifth and sixth panels) is normalized superposed epoch analysis results of >0.6 MeV and >2.0 MeV electron fluxes observed by GOES 15. The red curves give the mean values, and the blue lines represent the upper and lower quartiles. Figure 2 (seventh to ninth panels) shows the trapped electron flux measurements of POES 15, 16, 18, and 19 satellites in three energy channels (>30 keV, >100 keV, and >300 keV) after performing the time normalization during the duration of P_{dyn} pulses and bin averaging the fluxes. Incorporation of POES electron flux data enables us to pursue a comprehensive analysis of the dynamic responses of radiation belt electron population in a broad spatial extent.

As shown in Figure 2, before the arrival of the dynamic pressure pulse, on average both the solar wind parameters and radiation belt electron flux measurements show modest and steady levels without large variations.

The mean value is around 11 R_E for the magnetopause location and around zero for *Dst*. When P_{dyn} increases quickly at the zero superposed epoch time to form the dynamic pressure pulse, the magnetopause is compressed down to lower L shells and *Dst* increases slightly during the sudden storm commencement. In contrast, the mean IMF B_z remains around zero. The average electron fluxes also primarily stay at the prepulse levels until P_{dyn} starts approaching the peak value. Specifically, GOES observed electron fluxes of $>$ 0.6 MeV and $>$ 2.0 MeV channels start to decline about 1 h before the P_{dyn} reaches its maximum value. The observations of POES satellites illustrate energy-dependent responses of radiation belt electron fluxes to the occurrence of the pressure pulse [e.g., *Xiong et al.*, 2015; *Reeves et al.*, 2016], showing that $>$ 30 keV and $>$ 100 keV electron fluxes increase and extend to both lower and higher L shells, while $>$ 300 keV electron fluxes decrease to a small degree at $L \sim 6$ and predominantly extend to lower L shells. Following the pressure pulse, P_{dyn} starts to decrease quickly and the magnetopause location moves outward. Correspondingly, GOES electron fluxes continue to decay for several hours and subsequently increase for recovery to the prepulse levels. The timescales for both flux decay and recovery are much shorter for electrons $>$0.6 MeV than $>$2.0 MeV. POES observations show more complex behavior. At energies $>$30 keV, electron fluxes show the drop at $L > \sim 7$, but the increase at $L < \sim 6$ and the extension to lower L shells $\sim L = 3$. The $>$100 keV electron fluxes show the temporal variation in a manner similar to that of $>$30 keV electrons, while fluxes are confined to a slightly different range of L shell. The major feature of $>$300 keV electron fluxes is that they decrease in a few hours right after the pressure pulse and then quickly increase to the prepulse levels.

On the basis of normalized superposed epoch analysis, the average features of radiation belt electron fluxes with respect to the entire course of a solar wind dynamic pressure pulse (i.e., "−1"–"+2" days) in Figure 2 manifest an overall strong dependence of electron radiation belt variation on energy, L shell, and time. However, Figure 2 cannot look into the underlying connections between the radiation belt electron dynamics and various potentially important parameters during the course of a pressure pulse. A number of studies have emphasized the effect of different solar wind parameters upon radiation belt electron flux dropouts in the magnetosphere [e.g., *Yuan and Zong*, 2013; *Gao et al.*, 2015]. In the present study, we will follow those studies to statistically validate their conclusions and to investigate in detail the impact of important solar wind and magnetospheric parameters on the dynamic responses of electron radiation belt during solar wind dynamic pressure pulses.

Figure 3 shows the normalized superposed epoch analysis results for 10 pressure pulse events with the largest average northward IMF B_z (left column) and 10 pressure pulse events with the largest average southward IMF B_z (right column). Such a large difference in IMF B_z is clearly illustrated in Figure 3 (second row). Conditions of significantly northward IMF B_z are more likely to correspond to sharper increases in P_{dyn} and sudden storm commencements, while conditions of significantly southward IMF B_z are preferentially associated with the storm main phase and lower magnetopause location. By comparison, there are a number of interesting features of radiation belt electron flux variations under the above two distinct conditions: (1) relativistic electron fluxes observed by GOES 15 increase slightly as the pulse occurs and start to decrease quickly around 1–2 h before the P_{dyn} peak of the pulse for the most northward IMF B_z events. But for the most southward IMF B_z events, GOES observed electron fluxes are more likely to decrease following the occurrence of the pulse, especially for $>$ 0.6 MeV electrons; (2) during the course of the pressure pulse, POES satellites observe a slight increase in average radiation belt electron fluxes for $>$30 keV and $>$100 keV energy channels under both conditions of significantly northward and southward IMF B_z, while for $>$300 keV electrons, POES satellites observe flux increase for the most northward IMF B_z events but flux decrease for the most southward IMF B_z events; (3) after the peak of the pressure pulse, POES satellites see the electron flux decreases at higher L shells regardless of energy channel or IMF B_z condition. Note that L shells for flux decrease go lower as electron energy increases. For the most southward IMF B_z events, POES observed electron fluxes in the outer radiation belt increase quickly right after the pressure pulse and substantially exceed the prepulse level during the phase of pressure decrease and magnetospheric recovery. In contrast, for the most northward IMF B_z events, POES observed electron fluxes increase to a lesser extent for $>$30 keV and $>$100 keV energy channels but first decrease considerably and then increase gradually for $>$300 keV electrons; (4) overall, POES measurements indicate that for the two conditions of IMF B_z, average radiation belt energetic electron fluxes are larger under conditions of most northward IMF B_z before the occurrence of the pulse, become comparable during the pulse period, and are larger under conditions of most southward IMF B_z after the completion of the pulse. In addition, large electron fluxes can well extend to lower L shells for

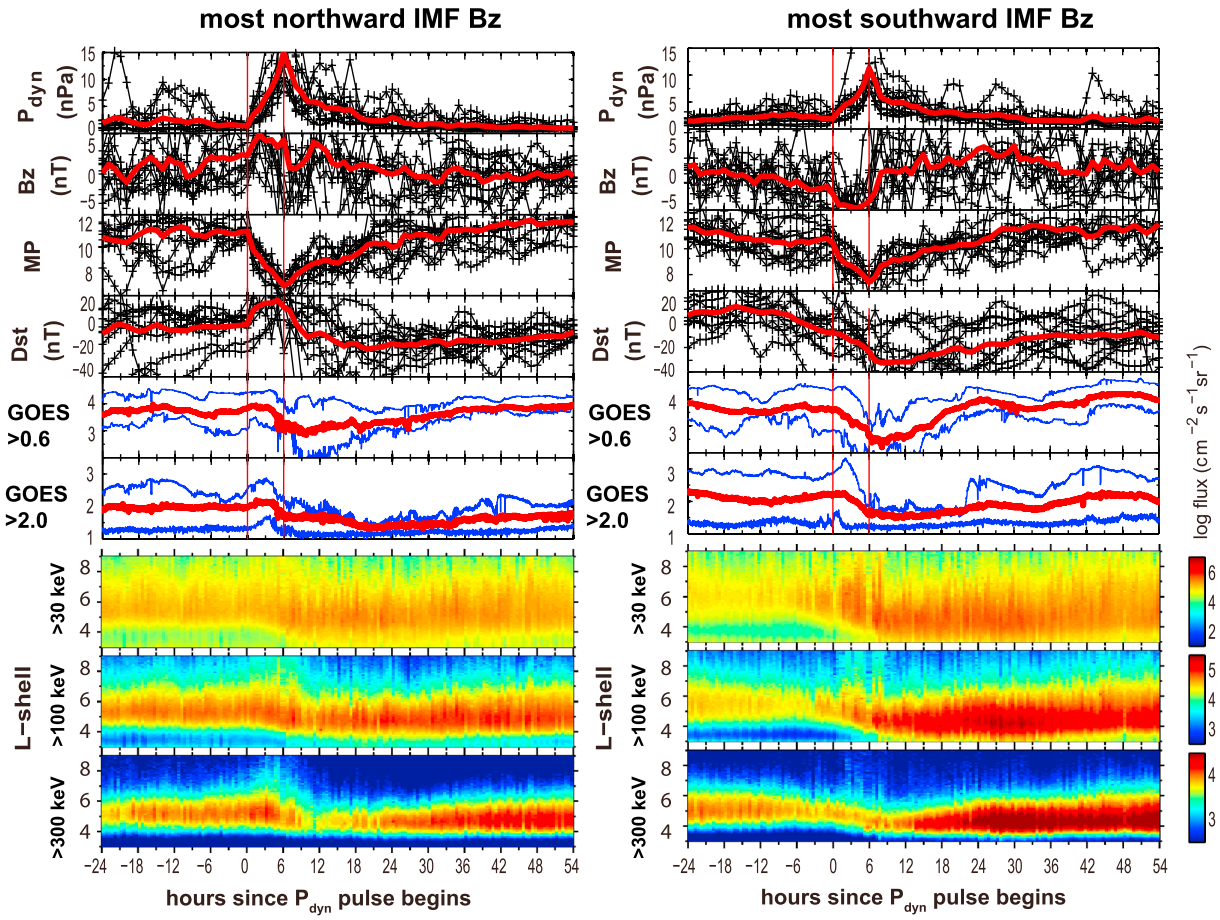

Figure 3. Same as in Figure 2 except for 10 events with the largest average northward IMF B_z versus 10 events with the largest average southward IMF B_z.

the most southward IMF B_z events. These features demonstrate the complex interplay of various underlying physical processes upon the dynamic responses of radiation belt electron fluxes to solar wind dynamic pressure pulse events. Further discussions of these results and the aforementioned results from the perspective of physical understanding are deferred to section 4.

Figure 4 shows the normalized superposed epoch analysis results for 10 events with the lowest magnetopause position (left column) and 10 events with the highest magnetopause position (right column). For the lowest magnetopause position events, the minimum magnetopause position is around 7 *Re*, while for the highest magnetopause position events, it is around 8 *Re*. The striking differences in P_{dyn} and magnetopause position are clearly illustrated in Figure 4 (first and second rows). In addition, the direction of IMF B_z is also distinct between these two groups of events. During the lowest magnetopause events, IMF B_z stays southward for a longer period, and *Dst* decreases considerably during the P_{dyn} pulse and after the P_{dyn} peak. It is apparent that intense P_{dyn} jumps and southward IMF B_z is favorable to result in the strong compression of the magnetosphere and the marked inward intrusion of the magnetopause, manifesting a likely coupling of these two parameters to affect the effect of magnetopause location on the pulse-associated radiation belt electron dynamics.

By comparison, there are a number of interesting features of radiation belt electron flux variations under the above two distinct conditions. First, the average radiation belt electron fluxes at the geostationary orbit are considerably smaller for the events with lower magnetopause location than for higher magnetopause location before the solar wind dynamic pressure pulse. It is therefore suggested that the preconditioned electron flux profile should be an important contributor to the radiation belt electron dynamic responses to pressure pulses, which will be evaluated more carefully in Figure 6. Fluxes of >0.6 MeV electrons observed by GOES 15 reduce quickly after the pulse under lowest magnetopause position conditions, but for the highest

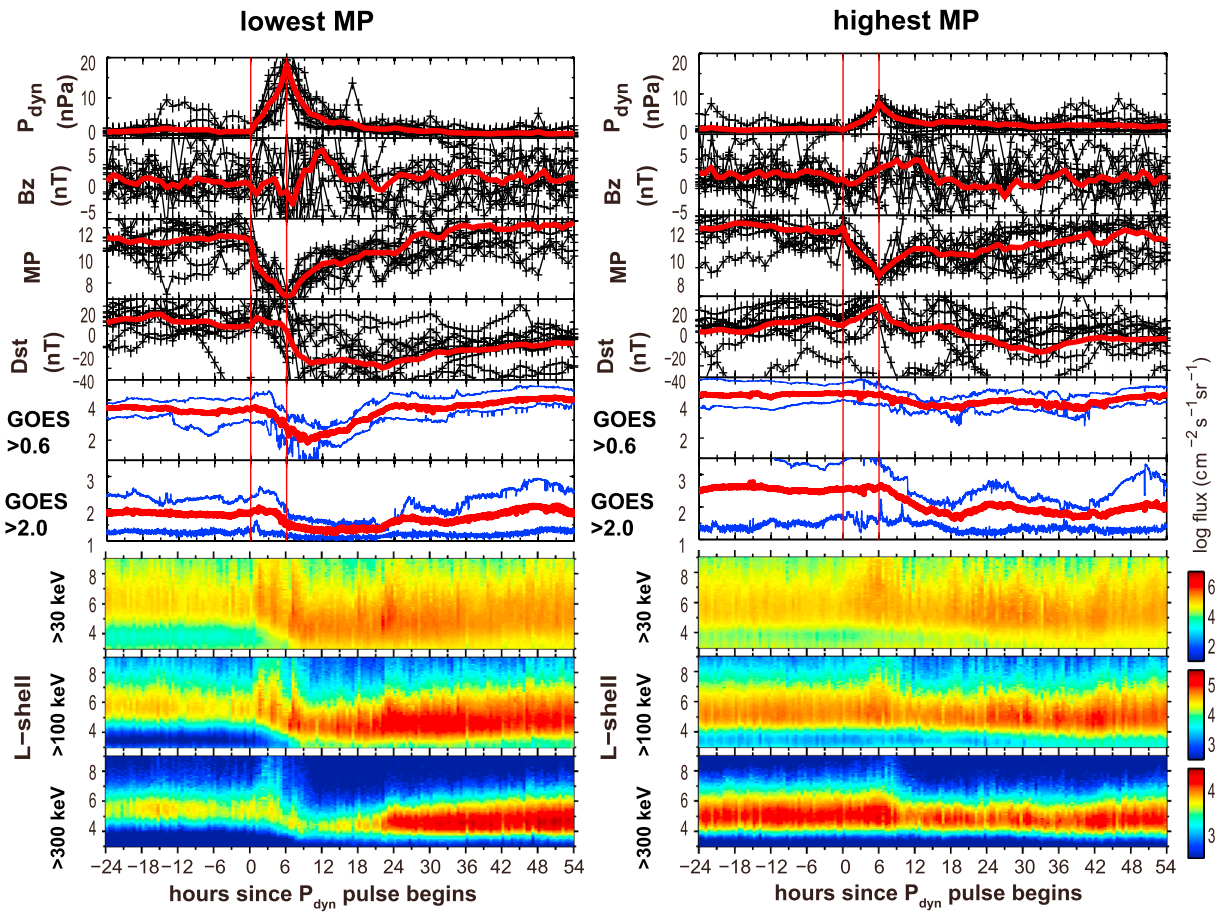

Figure 4. Same as in Figure 2 except for 10 events with the lowest magnetopause position versus 10 events with the highest magnetopause position.

magnetopause position events, GOES 15 only observes slight decay after the P_{dyn} pulse. Fluxes of >2.0 MeV electrons decay by about an order of magnitude after the P_{dyn} pulse for both groups of pulse events, but they decrease much faster when the magnetopause experiences a deeper inward penetration, approaching the minimum around 12 h after the zero epoch time. Second, during the pressure rise period, injections of >30 keV and >100 keV electrons at higher L shells are apparently more intense under lowest magnetopause location conditions. After the peak of the pressure pulse, POES satellites see the electron flux decrease at higher L shells regardless of energy channel or magnetopause position. For the lowest magnetopause position events, POES satellites observe average flux dropouts at $L>5$ for >300 keV electrons, which however is seen at $L>6$ for the highest magnetopause position events. Third, GOES and POES combined measurements suggest that radiation belt electron fluxes under conditions when the magnetopause is most compressed, are lower before the occurrence of the pressure pulse, decrease quicker and penetrate inward deeper during the electron flux dropout period, and recover to or even exceed prepulse levels faster than for the events with weaker magnetopause compression.

Figure 5 shows the normalized superposed epoch analysis results for 10 events with smallest values of $(Dst)_{min}$ (left column) and 10 events with largest values of $(Dst)_{min}$ (right column). The average $(Dst)_{min}$ is around -60 nT for the former and ~ -10 nT for the latter. The average profiles of P_{dyn} and magnetopause position are similar for both event groups during the normalized period of the pressure pulse, while the IMF B_z is primarily southward and the magnetopause is more compressed for the smallest $(Dst)_{min}$ events. Large electron flux decays are seen from the GOES measurements at the two energy channels during the course of the pressure pulse, but the events with smallest $(Dst)_{min}$ produce more intense flux decreases, which emerge during the P_{dyn} elevation phase but before the peak. POES trapped electron measurements also show dynamic flux variations at all the three energy channels. Overall, for the pulse events with large

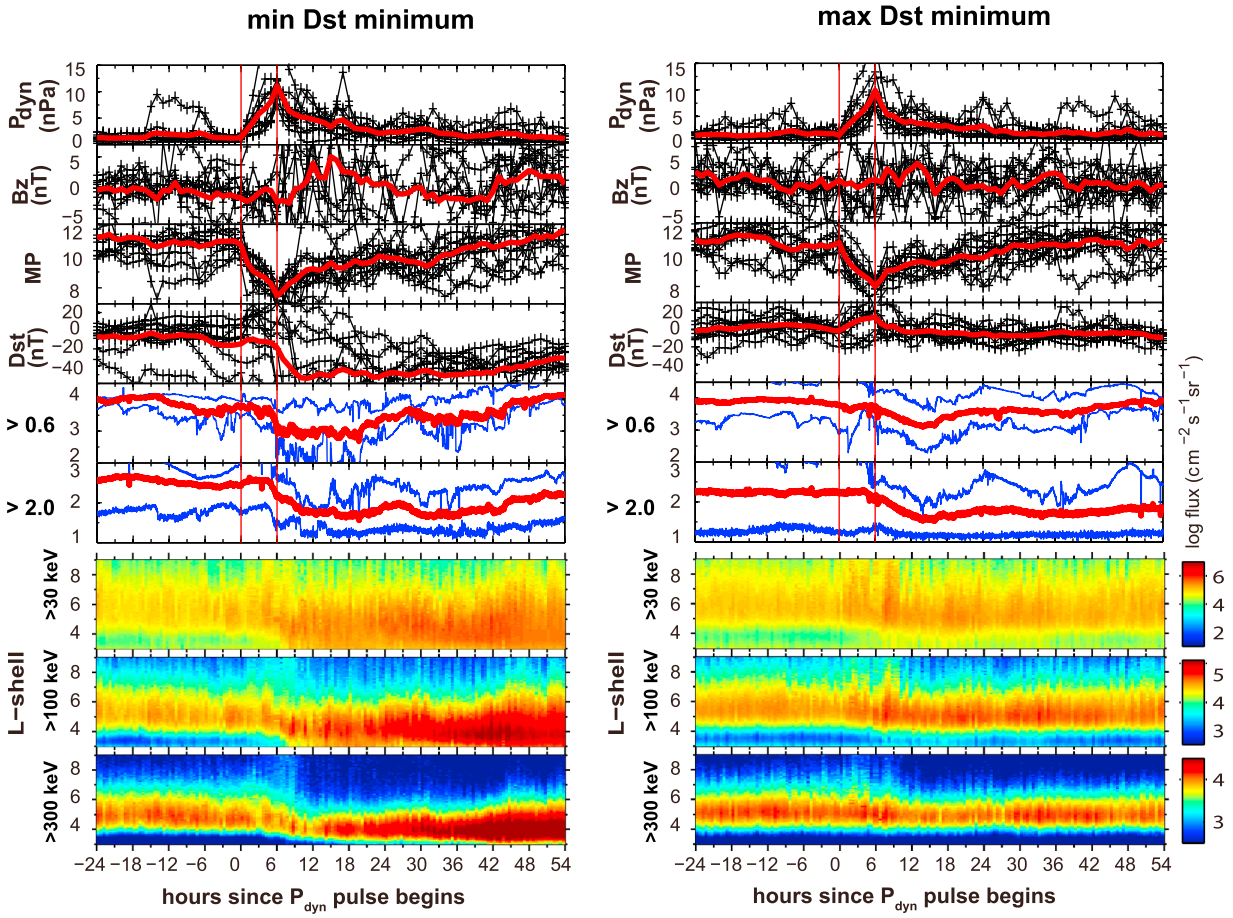

Figure 5. Same as in Figure 2 except for 10 events with the smallest values of $(Dst)_{min}$ versus 10 events with the largest values of $(Dst)_{min}$.

negative values of $(Dst)_{min}$, radiation belt electrons respond to in a manner similar to those with southward IMF B_z, that is, largest decay occurring after the P_{dyn} peak and subsequent (postpulse) remarkable recovery exceeding the prepulse level. The latter can even extend to $L \sim 3$. In contrast, electron flux dropouts become much less significant when the absolute magnitude of $(Dst)_{min}$ becomes smaller.

To evaluate the degree of electron flux decay in the outer radiation belt, we define a geostationary dropout index, which is evaluated as the ratio of the minimum of GOES > 2.0 MeV electron flux in the 48 h after zero epoch time to the mean value of GOES > 2.0 MeV electron flux in the 24 h before zero epoch time. Figure 6 gives normalized superposed epoch analysis results for 10 events with the smallest dropout index of GOES >2.0 MeV electron fluxes (left column) and 10 events with the largest dropout index of GOES >2.0 MeV electron fluxes (right column). It is indicated that when the geostationary dropout indices are large, POES electron fluxes show much more pronounced decays around the heart of the outer radiation belt during and following the pressure pulse. It is also worthwhile to note that for the pulse events of largest geostationary dropout index, the preconditioned (i.e., prepulse) fluxes of >100 keV and >300 keV electrons are significantly stronger and cover a broader L shell range. However, the largest ratio of electron flux increase before and after the pulse occurs under the circumstances of preconditioned low electron fluxes.

Figure 7 displays the normalized superposed epoch analysis results for 10 events with longest P_{dyn} rise time (left column) and 10 events with shortest P_{dyn} rise time (right column). The IMF B_z of events with longest P_{dyn} rise time turns northward after the P_{dyn} pulse and then turns southward. But for shortest P_{dyn} rise time events, IMF B_z remains primarily unchanged during the entire time interval. It is clearly demonstrated from the measurements of GOES 15 and POES satellites that the solar wind dynamic pressure pulse with longer P_{dyn} rise time can cause radiation belt electron flux decay in a quicker and stronger manner. Besides the pressure pulse duration, its magnitude is also important to electron flux variations. The studies of *Shprits et al.* [2012] and *Ni et al.* [2013a]

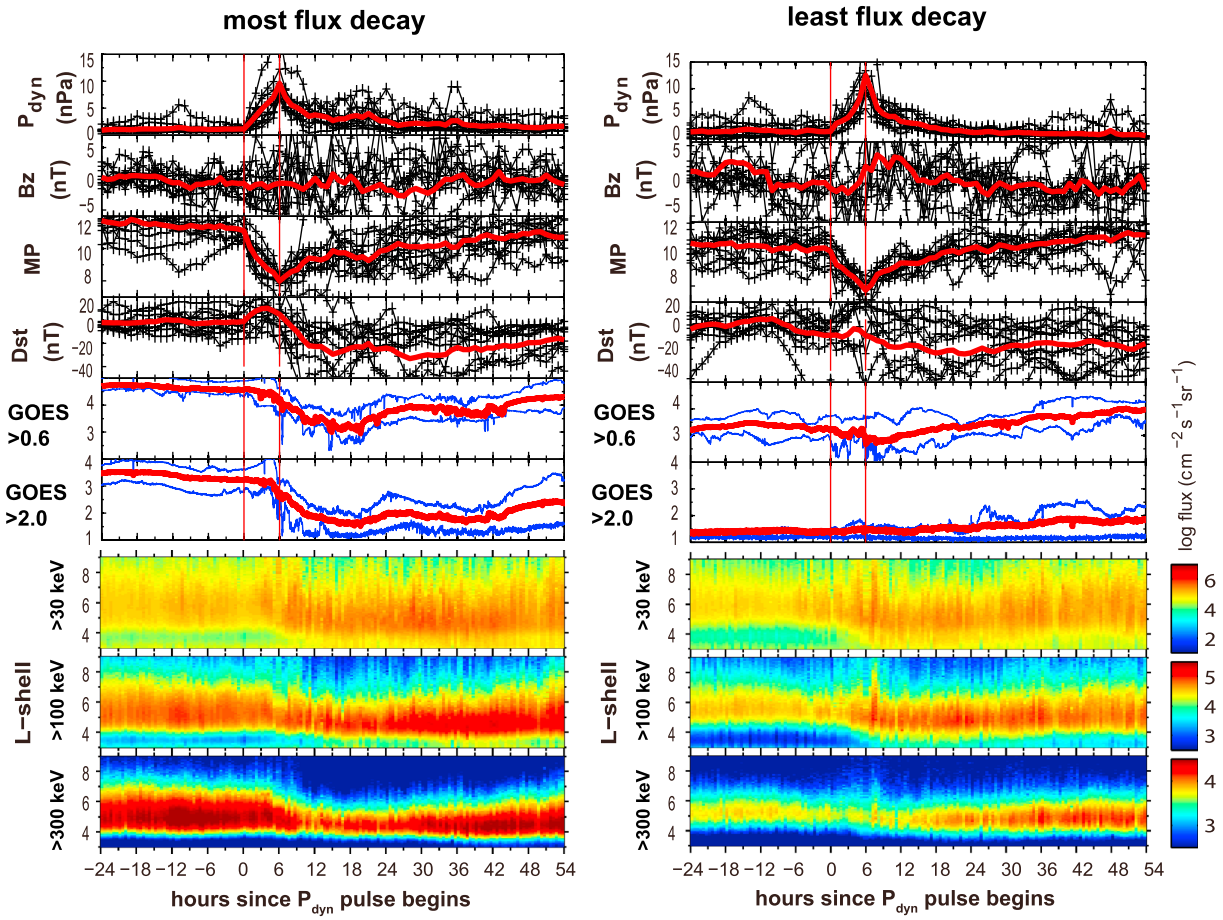

Figure 6. Same as in Figure 2 except for 10 events with the largest geostationary dropout index of GOES > 2.0 MeV electron fluxes versus 10 events with the smallest geostationary dropout index of GOES > 2.0 MeV electron fluxes.

investigated comprehensively the effect of the pressure pulse magnitude to find that flux dropout events can occur with higher possibility for larger magnitude P_{dyn} pulses.

4. Discussions

Former studies indicated that electron flux dropout could be dominated by a combination of magnetopause shadowing and/or atmospheric loss (see reviews by *Shprits et al.* [2008b], *Turner et al.* [2014a, 2014b], *Ni et al.* [2013b], and *Xiang et al.* [2016]). In the present study, our results further support that these mechanisms contribute to the radiation belt electron dynamic behaviors alone or in combination at different phases of a solar wind dynamic pressure pulse. As shown in Figure 3, corresponding to most northward IMF B_z conditions, when P_{dyn} drops from the peak value and the magnetopause recovers to a high location, electron fluxes at $L < 6$ exhibit significant decreases, which can be a consequence of strong outward radial diffusion following the loss process to the magnetopause. In contrast, for most southward IMF B_z conditions, electron fluxes at $L < 6$ undergo substantial decreases during the P_{dyn} elevation period. Taken into account that magnetospheric wave activities are preferentially intensified during periods of southward IMF B_z, it is reasonable to suggest that wave-induced pitch angle scattering can contribute to the flux decrease arising from loss to the atmosphere. Such wave candidates include whistler-mode chorus, plasmaspheric hiss, and electromagnetic ion cyclotron (EMIC) waves, whereas these wave modes tend to predominantly resonate with radiation belt electrons at different energies from ~ 1 keV to 10 MeV. A recent simulation of *Kang et al.* [2016], on the basis of the Radiation Belt Environment (RBE) model [*Fok et al.*, 2008], demonstrated that EMIC waves can cause efficient electron flux dropouts in the heart of the radiation belt within a short time period. *Xiang et al.* [2016] looked into multisatellite simultaneous observations of magnetopause and atmospheric losses of radiation belt electrons during an event

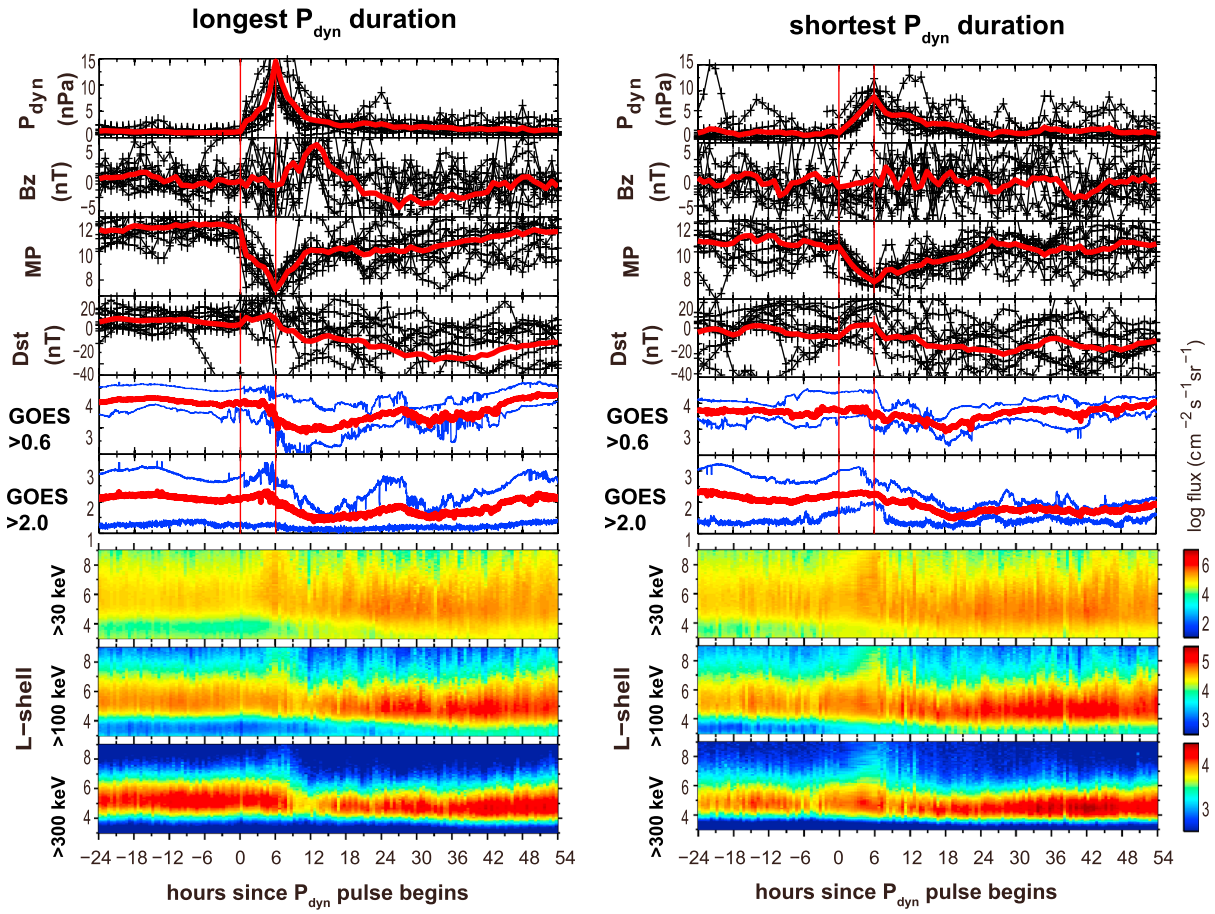

Figure 7. Same as in Figure 2 except for 10 events with longest P_{dyn} rise time versus 10 events with shortest P_{dyn} rise time.

of intense solar wind dynamic pressure pulse. They also found that electron scattering by plasma waves should play as an important mechanism to explain the measured real electron losses in the outer zone. Quantitative analyses of wave-induced scattering and resultant loss processes are outside the scope of the present study, which, however, certainly requires comprehensive investigation in the future.

In the present study 40 events are used for detailed analyses and split into different classifications grouped by 10 events of various parameters. While it is difficult to evaluate to which extent this investigation represents the statistical features of the dynamic responses of radiation belt electron fluxes during the period of solar wind dynamic pressure pulse, we argue that our methodology of event selection and data treatment has followed a number of previous similar investigations. For instance, *Hietala et al.* [2014] used the same method to study the depleting effects of 31 ICME-driven sheath regions on the outer electron radiation belt for the solar cycle 23. They classified the events into specific groups and then compared the 10 events with largest value of the respective parameter to the 10 events exhibiting the lowest value in that parameter. *Li et al.* [2015] also investigated 16 efficient radiation belt electron acceleration and 17 inefficient acceleration events during the period from October 2012 to March 2015 to study the potential solar wind conditions leading to efficient electron acceleration. In addition, *Yuan and Zong* [2013] analyzed 45 CME-associated solar wind dynamic pressure enhancement events during the period of 1998–2003 to look into the outer zone relativistic electron flux dropouts under different solar wind conditions. According to those previous studies, our investigation on basis of 40 robust pressure pulse events in 28 months is reasonable to produce useful results regarding the pressure pulse-associated dynamic responses of the radiation belts. On the other hand, all those previous studies performed superposed epoch analyses in a conventional manner, our present study adopts the normalized superposed epoch analysis by using multiple markers rather than only one marker; therefore, it is expected that further details of radiation belt electron flux variation can be retained and that specific features on a similar timeline can be identified to link underlying drivers during events.

There are cases that radiation belt electron fluxes show almost no changes during the course of a P_{dyn} pulse [e.g., *Shprits et al.*, 2012; *Ni et al.*, 2013a], and there are also cases in which they exhibit dramatic decreases during weak geomagnetic storms [e.g., *Anderson et al.*, 2015]. Such complexity in the radiation belt electron responses is further expressed by our results. As shown in Figure 5, a combination of P_{dyn} pulse and moderate geomagnetic storm tends to provide a favorable condition for radiation belt electron flux dropouts. In contrast, weak *Dst* activities are likely to drive much smaller electron losses. The explanations to these differences are manifold, including the "*Dst* effect," wave-particle interactions, and magnetopause shadowing. It is also strongly suggested that the prompt, substantial postpulse electron flux increase that well exceeds the prepulse levels during more intense *Dst* activities is closely correlated with the considerable accumulation (i.e., injection) of tens of keV electrons.

Another interesting result obtained in this study is that the radiation belt preconditioning also contributes importantly to the responses of radiation belt electron flux to solar wind dynamic pressure pulse events (see Figure 6). Our results clearly demonstrate that pulse-associated electron flux dropouts prefer to occur when preconditioned (i.e., prepulse) electron fluxes are high and that more pronounced electron flux enhancements exceeding the prepulse levels are likely to take place when preconditioned electron fluxes are low. Solid consistency between the variations of relativistic electron flux at the geostationary orbit and of energetic electron flux around the heart of the outer zone can be also registered.

Overall, our results, on the basis of a comprehensive analysis of multiyear electron flux data from both geosynchronous and low-altitude satellites, provide further quantitative information concerning the electron radiation belt responses before, during, and following the occurrences of solar wind dynamic pressures. They also release important clues of physical processes/drivers involved in the loss, acceleration, and transport of radiation belt electrons under various solar wind and geomagnetic conditions and preconditions in the electron radiation belts. Therefore, the present study has implications for our use to develop a module to radiation belt modeling codes that help better simulate and predict radiation belt electron flux dropouts. This will be a topic for future study.

5. Conclusions

In this paper we have investigated in detail the radiation belt electron flux variations under a variety of solar wind and magnetospheric conditions by performing a normalized superposed epoch analysis of over 2 years of electron data measured by GOES 15 and four POES satellites. Normalized superposed epoch analysis is able to place specific features on a similar timeline to look into the underlying connections and potential drivers during events. Our major conclusions are summarized as follows:

1. In a statistically average sense, radiation belt electron fluxes at tens of keV tend to increase during the period of P_{dyn} jump. In contrast, $>$100 keV radiation belt electron fluxes exhibit large depletions right after the P_{dyn} peak rather than during the pulse, especially during the conditions of northward IMF B_z. Under southward IMF B_z conditions, electron flux dropouts are more likely to occur during the P_{dyn} pulse to cover a broad range of L shell, and afterward, the fluxes recover markedly to exceed the prepulse level to a degree apparently larger than that for northward IMF B_z conditions.
2. Inward intrusion of the magnetopause location, under the impact of solar wind dynamic pressure enhancements and the direction of IMF B_z, plays a critical role in the dynamic responses of radiation belt electrons. Deeper earthward magnetopause erosion provides favorable circumstances for the prompt occurrence of electron flux dropouts at spatial extents down to $L \sim 5$.
3. For pulse events with large negative values of $(Dst)_{min}$, radiation belt electrons respond in a manner similar to those with southward IMF B_z, that is, the largest decay occurring after the P_{dyn} peak and subsequent (postpulse) remarkable recovery exceeding the prepulse level. The latter can even extend to $L \sim 3$. Electron flux dropouts become more significant when the magnitude of $(Dst)_{min}$ decreases largely. The pressure pulses with longer duration also tend to produce quicker and stronger electron flux decay.
4. The precondition of radiation belt electron fluxes also contribute to their dynamic variations during and following solar wind dynamic pressure pulses. The events with high electron fluxes before the P_{dyn} pulse tend to experience more severe electron flux dropouts during the course of the pulse. But the largest ratio of electron flux increase before and after the pulse occurs under the preconditioned low electron fluxes.

Acknowledgments

This work was supported by NSFC grants 41204120, 41474141, 41304130, and 41574160, the Projects funded by China Postdoctoral Science Foundation (2013 M542051 and 2014 T70732), and the Project supported by the Specialized Research Fund for State Key Laboratories. GOES data were obtained from http://satdat.ngdc.noaa.gov/sem/goes/, POES MEPED data were obtained from ftp://satdat.ngdc.noaa.gov/sem/poes/, and the solar wind parameters and geomagnetic activity indices were obtained from the NASA OmniWeb (http://cdaweb.gsfc.nasa.gov).

References

Anderson, B. R., R. M. Millan, G. D. Reeves, and R. H. W. Friedel (2015), Acceleration and loss of relativistic electrons during small geomagnetic storms, *Geophys. Res. Lett.*, *42*, 10,113–10,119, doi:10.1002/2015GL066376.

Baker, D. N., S. G. Kanekal, X. Li, S. P. Monk, J. Goldstein, and J. L. Burch (2004), An extreme distortion of the Van Allen belt arising from the 'Halloween' solar storm in 2003, *Nature*, *432*, 878–881, doi:10.1038/nature03116.

Borovsky, J. E., and M. H. Denton (2009), Relativistic-electron dropouts and recovery: A superposed epoch study of the magnetosphere and the solar wind, *J. Geophys. Res.*, *114*, A02201, doi:10.1029/2008JA013128.

Casadio, S., and O. Arino (2011), Monitoring the South Atlantic anomaly using ATSR instrument series, *Adv. Space Res.*, *48*(6), 1056–1066, doi:10.1016/j.asr.2011.05.014.

Evans, D. S., and M. S. Greer (2004), Polar Orbiting Environmental Satellite Space Environment Monitor-2: Instrument descriptions and archive data documentation, NOAA Tech. Mem. 93, version 1.4, Space Weather Predict. Cent., Boulder, Colo.

Fok, M.-C., R. B. Horne, N. P. Meredith, and S. A. Glauert (2008), Radiation Belt Environment model: Application to space weather nowcasting, *J. Geophys. Res.*, *113*, A03S08, doi:10.1029/2007JA012558.

Gao, X., W. Li, J. Bortnik, R. M. Thorne, Q. Lu, Q. Ma, X. Tao, and S. Wang (2015), The effect of different solar wind parameters upon significant relativistic electron flux dropouts in the magnetosphere, *J. Geophys. Res. Space Physics*, *120*, 4324–4337, doi:10.1002/2015JA021182.

Green, J. C. (2013), *MEPED Telescope Data Processing Algorithm Theoretical Basis Document*, Natl. Oceanic and Atmos. Admin. Space Environ. Cent., Boulder, Colo.

Hietala, H., E. K. J. Kilpua, D. L. Turner, and V. Angelopoulos (2014), Depleting effects of ICME-driven sheath regions on the outer electron radiation belt, *Geophys. Res. Lett.*, *41*, 2258–2265, doi:10.1002/2014GL059551.

Hwang, J., E.-J. Choi, J.-S. Park, M.-C. Fok, D.-Y. Lee, K.-C. Kim, D.-K. Shin, M. E. Usanova, and G. D. Reeves (2015), Comprehensive analysis of the flux dropout during 7–8 November 2008 storm using multisatellite observations and RBE model, *J. Geophys. Res. Space Physics*, *120*, 4298–4312, doi:10.1002/2015JA021085.

Kang, S.-B., M.-C. Fok, A. Glocer, K.-W. Min, C.-R. Choi, E. Choi, and J. Hwang (2016), Simulation of a rapid dropout event for highly relativistic electrons with the RBE model, *J. Geophys. Res. Space Physics*, *121*, 4092–4102, doi:10.1002/2015JA021966.

Katus, R. M., M. W. Liemohn, D. L. Gallagher, A. Ridley, and S. Zou (2013), Evidence for potential and inductive convection during intense geomagnetic events using normalized superposed epoch analysis, *J. Geophys. Res. Space Physics*, *118*, 181–191, doi:10.1029/2012JA017915.

Lam, M. M., R. B. Horne, N. P. Meredith, S. A. Glauert, T. Moffat-Griffin, and J. C. Green (2010), Origin of energetic electron precipitation $>$ 30 keV into the atmosphere, *J. Geophys. Res.*, *115*, A00F08, doi:10.1029/2009JA014619.

Li, W., R. M. Thorne, J. Bortnik, D. N. Baker, G. D. Reeves, S. G. Kanekal, H. E. Spence, and J. C. Green (2015), Solar wind conditions leading to efficient radiation belt electron acceleration: A superposed epoch analysis, *Geophys. Res. Lett.*, *42*, 6906–6915, doi:10.1002/2015GL065342.

Ni, B., Y. Shprits, T. Nagai, R. Thorne, Y. Chen, D. Kondrashov, and H.-J. Kim (2009a), Reanalyses of the radiation belt electron phase space density using nearly equatorial CRRES and polar-orbiting Akebono satellite observations, *J. Geophys. Res.*, *114*, A05208, doi:10.1029/2008JA013933.

Ni, B., Y. Shprits, R. Thorne, R. Friedel, and T. Nagai (2009b), Reanalysis of relativistic radiation belt electron phase space density using multisatellite observations: Sensitivity to empirical magnetic field models, *J. Geophys. Res.*, *114*, A12208, doi:10.1029/2009JA014438.

Ni, B., Y. Y. Shprits, R. Friedel, R. M. Thorne, M. Daae, and Y. Chen (2013a), Responses of Earth's radiation belts to solar wind dynamic pressure variations in 2002 analyzed using multi-satellite data and Kalman filtering, *J. Geophys. Res. Space Physics*, *118*, 4400–4414, doi:10.1002/jgra.50437.

Ni, B., J. Bortnik, R. M. Thorne, Q. Ma, and L. Chen (2013b), Resonant scattering and resultant pitch angle evolution of relativistic electrons by plasmaspheric hiss, *J. Geophys. Res. Space Physics*, *118*, 7740–7751, doi:10.1002/2013JA019260.

Ni, B., et al. (2015), Resonant scattering of outer zone relativistic electrons by multiband EMIC waves and resultant electron loss time scales, *J. Geophys. Res. Space Physics*, *120*, 7357–7373, doi:10.1002/2015JA021466.

Reeves, G. D., et al. (2016), Energy-dependent dynamics of keV to MeV electrons in the inner zone, outer zone, and slot regions, *J. Geophys. Res. Space Physics*, *121*, 397–412, doi:10.1002/2015JA021569.

Shprits, Y. Y., R. M. Thorne, R. Friedel, G. D. Reeves, J. Fennell, D. N. Baker, and S. G. Kanekal (2006), Outward radial diffusion driven by losses at magnetopause, *J. Geophys. Res.*, *111*, A11214, doi:10.1029/2006JA011657.

Shprits, Y. Y., S. R. Elkington, N. P. Meredith, and D. A. Subbotin (2008a), Review of modeling of losses and sources of relativistic electrons in the outer radiation belts: I. Radial transport, *J. Atmos. Sol. Terr. Phys.*, *70*(14), 1679–1693, doi:10.1016/j.jastp.2008.06.008.

Shprits, Y. Y., D. A. Subbotin, N. P. Meredith, and S. R. Elkington (2008b), Review of modeling of losses and sources of relativistic electrons in the outer radiation belts: II. Local acceleration and loss, *J. Atmos. Sol. Terr. Phys.*, *70*(14), 1694–1713, doi:10.1016/j.jastp.2008.06.014.

Shprits, Y., M. Daae, and B. Ni (2012), Statistical analysis of phase space density buildups and dropouts, *J. Geophys. Res.*, *117*, A01219, doi:10.1029/2011JA016939.

Shue, J. H., J. K. Chao, H. C. Fu, C. T. Russell, P. Song, K. K. Khurana, and H. J. Singer (1997), A new functional form to study the solar wind control of the magnetopause size and shape, *J. Geophys. Res.*, *102*, 9497–9511, doi:10.1029/97JA00196.

Thorne, R. M. (2010), Radiation belt dynamics: The importance of wave-particle interactions, *Geophys. Res. Lett.*, *37*, L22107, doi:10.1029/2010GL044990.

Turner, D. L., S. K. Morley, Y. Miyoshi, B. Ni, and C.-L. Huang (2012a), *Outer Radiation Belt Flux Dropouts: Current Understanding and Unresolved Questions*, *Geophys. Monogr. Ser.*, vol. 199, edited by D. Summers, I. R. Mann, and D. N. Baker, pp. 195–212, AGU, Washington, D. C., doi:10.1029/2012GM001310.

Turner, D. L., Y. Shprits, M. Hartinger, and V. Angelopoulos (2012b), Explaining sudden losses of outer radiation belt electrons during geomagnetic storms, *Nat. Phys.*, *8*, 202–212, doi:10.1038/nphys2185.

Turner, D. L., et al. (2014a), On the cause and extent of outer radiation belt losses during the 30 September 2012 dropout event, *J. Geophys. Res. Space Physics*, *119*, 1530–1540, doi:10.1002/2013JA019446.

Turner, D. L., et al. (2014b), Competing source and loss mechanisms due to wave-particle interactions in Earth's outer radiation belt during the 30 September to 3 October 2012 geomagnetic storm, *J. Geophys. Res. Space Physics*, *119*, 1960–1979, doi:10.1002/2014JA019770.

Xiang, Z., et al. (2016), Multi-satellite simultaneous observations of magnetopause and atmospheric losses of radiation belt electrons during an intense solar wind dynamic pressure pulse, *Ann. Geophys.*, *34*, 493–509, doi:10.5194/angeo-34-493-2016.

Xiong, Y., L. Xie, Z. Pu, S. Fu, L. Chen, B. Ni, W. Li, J. Li, R. Guo, and G. K. Parks (2015), Responses of relativistic electron fluxes in the outer radiation belt to geomagnetic storms, *J. Geophys. Res. Space Physics*, *120*, 9513–9523, doi:10.1002/2015JA021440.

Yokoyama, N., and Y. Kamide (1997), Statistical nature of geomagnetic storms, *J. Geophys. Res.*, *102*, 14,215–14,222, doi:10.1029/97JA00903.

Yuan, C., and Q. Zong (2013), Relativistic electron flux dropout in the outer radiation belt under different solar wind conditions, *J. Geophys. Res. Space Physics*, *118*, 7545–7556, doi:10.1002/2013JA019066.